Interfacing a Topological Qubit with a Spin Qubit in a Hybrid Quantum System

Bo Li (李博),[1,2] Peng-Bo Li (李蓬勃),[1,*] Yuan Zhou (周原),[1] Jie Liu (刘杰),[1]
Hong-Rong Li (李宏荣),[1] and Fu-Li Li (李福利)[1]

[1] *Shaanxi Province Key Laboratory of Quantum Information and Quantum Optoelectronic Devices, Department of Applied Physics, Xi'an Jiaotong University, Xi'an 710049, China*
[2] *Department of Physics and Astronomy, Purdue University, West Lafayette, Indiana 47907, USA*

(Received 18 December 2018; revised manuscript received 12 March 2019; published 9 April 2019)

We present and analyze a hybrid quantum system that interfaces a Majorana-hosted semiconductor nanowire with a single nitrogen-vacancy (N-*V*) center via a magnetized torsional cantilever. We show that the torsional mode of the mechanical resonator can strongly couple to the Majorana qubit and the spin qubit simultaneously, which allows us to interface them for quantum-state conversion through a dark-state protocol. This work provides a promising interface between the topological qubit and the conventional spin qubit. This interface may have interesting applications in quantum information and computation.

DOI: 10.1103/PhysRevApplied.11.044026

I. INTRODUCTION

Majorana fermion quasiparticles (MFs) realized in condensed matter systems have attracted great interest in recent years [1–5], because they provide a very intriguing platform for quantum science and technology. The proposed realizations include $p_x + ip_y$ superconductors [6], edges of two-dimensional (2D) topological insulators [7], quantum Hall states at filling factor 5/2 [8], and one-dimensional (1D) semiconducting quantum wires with strong spin-orbit interactions [9–13]. In these systems, the spin-orbit coupled semiconductor wires with proximity-induced superconductivity are of particular interest for their simple architectures. For the 1D quantum nanowire, the MFs are predicated to localize through the competition between the superconducting proximity effect and the Zeeman splitting. Recently, several experiments aiming at establishing the existence of MFs have been reported [14–17]. Meanwhile, it has been shown that the Majorana qubits can be controlled by integrating with the conventional ones, such as the flux qubits and the spin qubits [18–23].

Topological qubits (TPs) are one of the most promising candidates for quantum computation due to their extreme robustness against local fluctuations. However, the technical challenges are considerable: (i) it is well known that braiding operations of MFs cannot generate a complete set of universal quantum logic gates required for quantum computation and (ii) it is still challenging to operate and readout the quantum states of the MFs. To overcome these problems, several types of hybrid quantum architectures coupling the topological qubits to the conventional ones have been proposed. One potential route is controlling the microscopic wave function of the superconductors, which allows the strong coupling between a topological qubit and a flux qubit or a mechanical oscillator [24–26]. Other promising schemes include utilizing the Aharonov-Casher effect [27–29] or the fractional Josephson effect [30–32]. So far, for all of these protocols, further experimental demonstrations are needed to verify their feasibility.

For the conventional qubits, nitrogen-vacancy (N-*V*) centers in diamond are more attractive due to their unique features, such as the fast microwave manipulation, optical preparation and detection, and long coherence time even at room temperature [33–35]. In recent years, there has been a considerable effort to integrate N-*V* centers in hybrid quantum systems, allowing the preparation of fantastic quantum states [36–41], design of quantum logic gates [42–46], and storage or transfer of quantum information [47–52]. To further explore the potential of hybrid quantum systems, it is very appealing to interface topological qubits with N-*V* centers coherently. Integrating the topological degrees of freedom with the complete gate operations of N-*V* spins could provide a promising multiqubit platform for quantum computation. However, the energy mismatch between these two kinds of qubits poses a major obstacle for their coupling.

In this paper, we consider a hybrid quantum device interfacing a topological qubit with a single N-*V* center via a magnetized torsional cantilever. The topological qubit under consideration is realized in a spin-orbit coupled semiconductor nanowire, which is embedded on top of an *s*-wave superconductor to form a semiconductor-superconductor heterostructure. Here,

*lipengbo@mail.xjtu.edu.cn

the torsional cantilever is realized by an individual single-walled nanotube (SWNT) with a nanosize magnet attached. This nanoscale mechanical structure enables us to combine an isolated N-V center with the strong spin-torsion couplings. Together with the strong topology-torsion couplings induced by the magneto-Josephson effect [53], the mechanical torsional mode can strongly couple to both the Majorana qubit and the N-V center. This enables coherent quantum-state conversion between the Majorana qubit and the spin qubit via a dark-state protocol. Owing to the topologically protected robustness and the universal quantum logic gates of N-V spins, there are more potential applications utilizing this hybrid architecture.

II. DESCRIPTION OF THE DEVICE

As shown schematically in Fig. 1, the hybrid quantum device under consideration consists of a topological qubit realized in a Majorana-hosted semiconductor nanowire, a magnetized torsional cantilever, and a single N-V center. The MFs in this architecture are realized in a spin-orbit coupled semiconductor nanowire with proximity-induced superconductivity. This 1D quantum nanowire could be driven to the topological phase regime and the MF exists as a quasiparticle at the boundary between the topological (T) and nontopological (N) regions [9–12]. Here, we divide the semiconductor nanowire into three sections to form a TNT junction [11,32] and define the topologically protected MFs as $\hat{\gamma}_{1/2/3/4}$.

In this setup, the magnetized torsional cantilever is realized by a nanomagnet with dimensions (l, w, t) suspended on a SWNT. Specifically, the individual SWNT works as

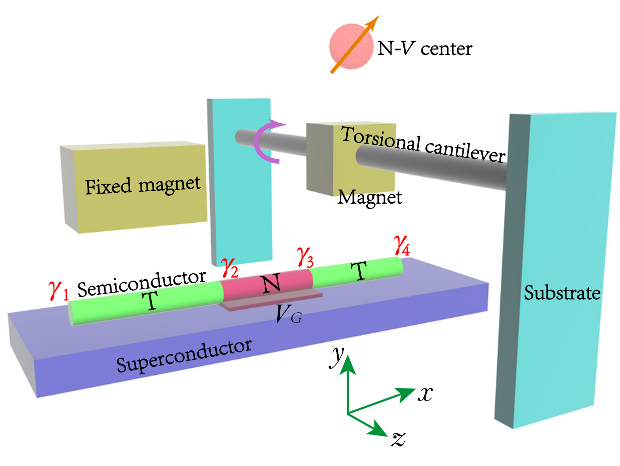

FIG. 1. Schematic of a hybrid quantum device interfacing a Majorana qubit and a single N-V center via a magnetized torsional cantilever. The spin-orbit coupled semiconductor nanowire is embedded on top of an s-wave superconductor and is divided into three regions to form a TNT junction. The MFs $\hat{\gamma}_{1/2/3/4}$ appear at the boundaries between the T and N regions. For the torsional cantilever, the individual SWNT works as a torsional spring for the suspended nanomagnet.

a torsional spring and mechanical support, which allows the suspended nanomagnet to rotate along the tube (z) axis (see Fig. 1). Without loss of generality, we assume that the nanomagnet can only rotate along the z axis with a small amplitude; then the Hamiltonian of the torsional cantilever reads $H_m = \frac{1}{2}I_z\omega_m^2\hat{\theta}^2 + \hat{L}^2/2I_z$, where ω_m, I_z, $\hat{L}$, and $\hat{\theta}$ are the torsional frequency, moment of inertia, angular momentum, and angular displacement, respectively. Similar to the canonical conjugate observable $\hat{X}$ and $\hat{P}$ of the center of mass mode, the rotational degree of freedom can be quantized [54] and the motion of the torsional cantilever can be described by the annihilation and creation operators as follows:

$$\hat{b} = \frac{1}{2}\left(\frac{\hat{\theta}}{\theta_{\text{ZPF}}} + \frac{i\hat{L}}{L_{\text{ZPF}}}\right), \quad \hat{b}^\dagger = \frac{1}{2}\left(\frac{\hat{\theta}}{\theta_{\text{ZPF}}} - \frac{i\hat{L}}{L_{\text{ZPF}}}\right), \quad (1)$$

where $L_{\text{ZPF}} = \sqrt{\hbar I_z\omega_m/2}$ and $\theta_{\text{ZPF}} = \sqrt{\hbar/(2I_z\omega_m)}$ denote the zero point fluctuations of the torsional mode.

A. MFs in 1D semiconductor nanowire

We first describe the 1D quantum nanowire hosting MFs. As shown in Fig. 1, the semiconductor nanowire is embedded on the top of an s-wave superconductor, and an external magnetic field $\vec{b} = b\vec{e}_z$ along the z axis is applied. There are two nanomagnets positioned straight above the nanowire: one is stationary in the left region and the other is free to vibrate in the right region. We assume that the magnetic fields induced by the two magnets are in the x-y plane, i.e., $\vec{B} = B\cos\theta\vec{e}_x + B\sin\theta\vec{e}_y$. We further use the angular displacement of the torsional cantilever to denote the relative field angle, which implies $\theta = \theta_r - \theta_l$.

The single-particle effective Hamiltonian for the semiconductor wire reads $H_0 = \hat{p}^2/2m^* - \mu + b\hat{\sigma}_z - \alpha(\hat{\vec{\sigma}} \times \hat{\vec{p}}) \cdot \hat{z}$ [9], where m^*, μ, b, and α are the effective mass, chemical potential, longitudinal magnetic field, and Rashba spin-orbit coupling strength, respectively. As a result of the proximity effect, the Cooper pairs tunneling into the nanowire can be described by the Hamiltonian $H_{\text{SC}} = \Delta e^{i\phi}\hat{\psi}_\uparrow^\dagger(x)\hat{\psi}_\downarrow^\dagger(x) + \text{H.c.}$, with $\Delta e^{i\phi}$ the proximity-induced gap. We now introduce the Nambu spinor basis $\hat{\Psi}^T = (\hat{\psi}_\uparrow, \hat{\psi}_\downarrow, \hat{\psi}_\downarrow^\dagger, -\hat{\psi}_\uparrow^\dagger)$ and model the 1D semiconductor nanowire with a Bogoliubov–de Gennes Hamiltonian

$$H = \frac{\hbar^2k^2}{2m^*}\hat{\tau}^z + \alpha k\hat{\tau}^z\hat{\sigma}^z - \mu\hat{\tau}^z + \Delta(\cos\phi\hat{\tau}^x - \sin\phi\hat{\tau}^y) - b\hat{\sigma}^z + B(\cos\theta\hat{\sigma}^x - \sin\theta\hat{\sigma}^y), \quad (2)$$

where the Pauli matrices $\hat{\sigma}^i$ and $\hat{\tau}^i$ represent the spin and particle-hole sectors, respectively.

As shown in Ref. [53], this semiconductor nanowire can be driven to the topological phase regime when $\Delta^2 - b^2 < B^2 - \mu^2$ and to the nontopological phase regime when

$\Delta^2 - b^2 > B^2 - \mu^2$ (considering only $\Delta^2 > b^2$). Note that Refs. [55,56] give similar results. In particular, the Bogoliubov operators of the quantum nanowire take a general form as $\hat{\gamma}_k = u_{k\uparrow}\hat{\psi}_{k\uparrow} + u_{k\downarrow}\hat{\psi}_{k\downarrow} + v_{k\uparrow}\hat{\psi}^\dagger_{-k\uparrow} + v_{k\uparrow}\hat{\psi}^\dagger_{-k\downarrow}$. For Majorana operators that satisfy $\hat{\gamma}_k^\dagger = \hat{\gamma}_k$, they may only occur in the momentum inversion symmetric condition $k \equiv -k$, i.e., $k = 0$. In the quantum nanowire, this indicates a phase boundary between the T and N regions [57].

The exactly zero-energy Majorana modes exist only in the ideal case where the two MFs possess an infinite distance. For a finite nanowire, the MFs gain a small energy as a result of the weak overlap of their wave functions. However, the wave functions are still well localized at the boundaries and we still have $\hat{\gamma}^\dagger \simeq \hat{\gamma}$ in general. Therefore, these MFs with nonzero energies can still be utilized to encode quantum information. We now denote the lengths of the three nanowire sections as $l_{l/m/r}$; then the MFs in the 1D semiconductor nanowire can be described by an effective low-energy Hamiltonian

$$\hat{H}_{\rm TP} = iE_l\hat{\gamma}_1\hat{\gamma}_2 + iE_m(\theta)\hat{\gamma}_2\hat{\gamma}_3 + iE_r\hat{\gamma}_3\hat{\gamma}_4, \tag{3}$$

where E_l, $E_m(\theta)$, and E_r are the coupling energies between the adjacent MFs.

B. Magneto-Josephson effect

To perform quantum-information processing with the topological degree of freedom, different ways to manipulate the MFs have been studied [58–62]. One potential route is to utilize the fraction Josephson effect [63,64]. Different from the conventional Josephson effect that allows tunneling by Cooper pairs only, the fraction Josephson effect supports single electron tunneling [32] and possess a 4π-periodic coupling energy [65]. Moreover, it has been shown that the magneto-Josephson effect can be used to realize the coherent coupling between the Majorana qubit and the magnetized torsional cantilever [53]. In particular, the spin current induced by the magneto-Josephson effect serves as a mechanical torque acting on the nanomagnet, which leads to the strong topology-torsion coupling.

For the TNT junction realized in the semiconductor nanowire, both the superconducting phases and the magnetic fields have contributions to the fractional Josephson effects. These contributions can be analyzed by the magnetism-superconductivity duality: if we interchange the magnetic terms $\{b, B, \theta, \hat{\sigma}^i\}$ with the superconducting terms $\{\mu, \Delta, \phi, \hat{\tau}^i\}$, the Hamiltonian in Eq. (2) takes the same form [55]. In a general case, the coupling interaction between $\hat{\gamma}_2$ and $\hat{\gamma}_3$ takes form as $E_M \propto E_M^0 \cos[(\theta_l - \theta_r)/2]\cos[(\phi_l - \phi_r)/2]$ [57]. In our system, we set the superconducting phases as the constants (i.e., $\phi_l = \phi_m = \phi_r$); then the coupling energy E_m can be tuned by changing the relative field angle θ.

To study the magneto-Josephson effect in the TNT junction, we now map the Bogoliubov–de Gennes Hamiltonian in Eq. (2) to the tight-binding model as follows:

$$\begin{aligned}\hat{H} = &-t\sum_{i,\sigma}\hat{c}^\dagger_{i\sigma}\hat{c}_{i+1\sigma} + \sum_{i,\sigma}(-2t + \mu_i + b_{i\sigma})\hat{c}^\dagger_{i\sigma}\hat{c}_{i\sigma}\\ &+ \alpha\sum_i(\hat{c}^\dagger_{i,\uparrow}\hat{c}_{i+1,\downarrow} - \hat{c}^\dagger_{i,\downarrow}\hat{c}_{i+1,\uparrow} + \text{H.c.})\\ &+ \sum_i(\Delta e^{i\phi}\hat{c}^\dagger_{i,\uparrow}\hat{c}^\dagger_{i,\downarrow} + \text{H.c.}) + \sum_i(Be^{i\theta}\hat{c}^\dagger_{i\uparrow}\hat{c}_{i,\downarrow} + \text{H.c.}).\end{aligned} \tag{4}$$

For this lattice version, $t = \hbar^2/(2m^*a^2)$ is the nearest-neighbor hopping strength, a is the lattice spacing constant, α is the spin-orbit coupling strength, $b_{i\uparrow/\downarrow} = \pm b$ is the Zeeman splitting, and $\hat{c}_{i\sigma}$ ($\hat{c}^\dagger_{i\sigma}$) is the annihilation (creation) operator of an electron with spin $\sigma = \uparrow$ ($\downarrow$).

We conduct numerical simulations by considering a 1D lattice model with 500 grid sites (300, 20, and 180 sites for the left, middle, and right regions, respectively). Here, the energy eigenvalues of the system are denoted as $\pm\varepsilon_i$, with the corresponding eigenstates $|\phi_{\pm\varepsilon_i}\rangle$. As shown in Figs. 2(a) and 2(b), the eigenstates $|\phi_{\pm\varepsilon_1}\rangle$ correspond to the excitations of $\hat{\gamma}_1$ and $\hat{\gamma}_4$, while the eigenstates $|\phi_{\pm\varepsilon_2}\rangle$ correspond to the excitations of $\hat{\gamma}_2$ and $\hat{\gamma}_3$. Theoretically, the isolated MFs can be obtained by combinations of these eigenstates in the limit $\varepsilon_{1,2} \simeq 0$, i.e., $|\phi_{\gamma_{1,4}}\rangle = (1/\sqrt{2})(|\phi_{\varepsilon_1}\rangle \pm |\phi_{\varepsilon_{-1}}\rangle)$ and $|\phi_{\gamma_{2,3}}\rangle = (1/\sqrt{2})(|\phi_{\varepsilon_2}\rangle \pm |\phi_{\varepsilon_{-2}}\rangle)$.

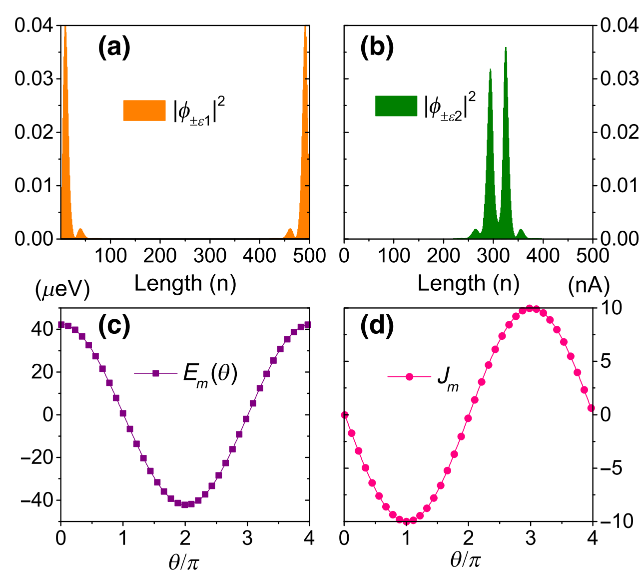

FIG. 2. (a) Edge modes $|\phi_{\pm\varepsilon_1}|^2$ of the lattice model, corresponding to MFs $\hat{\gamma}_1$ and $\hat{\gamma}_4$. (b) Edge modes $|\phi_{\pm\varepsilon_2}|^2$ of the lattice model, corresponding to MFs $\hat{\gamma}_2$ and $\hat{\gamma}_3$. (c) Hybridization energy $E_m(\theta)$ as a function of the relative field angle θ. (d) The spin current J_m induced by the magneto-Josephson effects.

Induced by the overlap of the edge states, the coupling energy between MFs decays exponentially with the separation [66]. According to Ref. [53], we now estimate the coupling energy $E_m(\theta)$ through the lowest-order perturbation theory and obtain

$$E_m(\theta) \approx \frac{|\langle \phi^0_{\gamma_2} e^{-i\theta_l/2\hat{\sigma}_z} | H | e^{i\theta_r/2\hat{\sigma}_z} \phi^0_{\gamma_3} \rangle|}{\sqrt{\langle \phi^0_{\gamma_2} | \phi^0_{\gamma_2} \rangle \langle \phi^0_{\gamma_3} | \phi^0_{\gamma_3} \rangle}}. \quad (5)$$

Then, we observe a 4π-periodic dependence between E_m and θ, as shown in Fig. 2(c). We also calculate the spin current passing through the middle region as $J_m = (e/\hbar)(\partial E^m(\theta)/\partial\theta)$ [67], and the result is shown in Fig. 2(d). The relevant parameters are based on InSb quantum wires, i.e., $m^* = 0.015\, m_e$, $\alpha = 0.2$ eVÅ, $a = 10$ nm, $\Delta = 0.5$ meV, and $g\mu_B = 1.5$ meV/T. Other parameters include $B = 200$ mT, $b = 200$ mT, and $\mu = 0$ meV for the topological regions and $B = 0$, $b = 200$ mT, and $\mu = -0.6$ meV for the nontopological region. Note that these parameters could be further optimized.

C. Topology-torsion couplings

We now discuss the coherent coupling between the Majorana qubit and the torsional motion. Firstly, we combine the MFs to construct two conventional Dirac fermions and obtain $\hat{f}_l = (\hat{\gamma}_1 + i\hat{\gamma}_2)/2$ and $\hat{f}_r = (\hat{\gamma}_3 + i\hat{\gamma}_4)/2$. Then, the two quantum states of the Dirac fermions, corresponding to the number of electrons on either side of the Josephson junction, can function as a physical topological qubit. These two states are denoted as $\hat{n}_x = \hat{f}_x^\dagger \hat{f}_x = 0$ or 1 $(x = l, r)$, with parity $\hat{P}_x = (-1)^{\hat{f}_x^\dagger \hat{f}_x} = \pm 1$. As braiding operations cannot change the total parity $\hat{P} = \hat{P}_l \hat{P}_r$ of the system, four MFs are usually needed to define a logical topological qubit [24,30]. We now define the topological qubit in the odd parity subspace and obtain $|\phi_{\mathrm{TP}}\rangle = c_1|0\rangle_l|1\rangle_r + c_2|1\rangle_l|0\rangle_r$. For this topological qubit, we also have [32]

$$i\hat{\gamma}_1\hat{\gamma}_2 \to -\hat{\sigma}^z_{\mathrm{TP}}, i\hat{\gamma}_2\hat{\gamma}_3 \to -\hat{\sigma}^x_{\mathrm{TP}}, i\hat{\gamma}_3\hat{\gamma}_4 \to \hat{\sigma}^z_{\mathrm{TP}}. \quad (6)$$

In this setup, it is the θ dependence of the hybridization energy $E_m(\theta)$ that leads to the strong topology-torsion coupling [53]. In particular, by expanding $E_m(\theta)$ in Eq. (3) around θ_0 to the first order, we arrive at $E_m(\theta) = E_m(\theta_0) + [\partial E_m(\theta)/\partial\theta]\theta_{\mathrm{ZPF}}(\hat{b}^\dagger + \hat{b})$. In what follows, we consider the case in which $E_m(\theta_0) \simeq 0$ [see Fig. 2(c)]; then the Hamiltonian of the topology-torsion dynamics has the form

$$\hat{H}_{\text{tor-TP}} = \hbar\omega_m \hat{b}^\dagger \hat{b} + \hbar\omega_{\mathrm{TP}}\hat{\sigma}^z_{\mathrm{TP}} - \hbar g(\hat{b}^\dagger + \hat{b})\hat{\sigma}^x_{\mathrm{TP}}, \quad (7)$$

where $\omega_{\mathrm{TP}} = (E_r - E_l)/\hbar$, and $g = (1/\hbar)[\partial E_m(\theta)/\partial\theta]\theta_{\mathrm{ZPF}}$ is the topology-torsion coupling strength. By tuning the hybridization energy E_l and E_r, we can steer the topology-torsion coupling to the near-resonance condition $\omega_{\mathrm{TP}} \simeq \omega_m$. Under the rotation-wave approximation, the topology-torsion dynamics can be described by

$$\hat{H}_{\text{tor-TP}} = \hbar\omega_m \hat{b}^\dagger \hat{b} + \hbar\omega_{\mathrm{TP}}\hat{\sigma}^z_{\mathrm{TP}} - \hbar g(\hat{b}^\dagger \hat{\sigma}^-_{\mathrm{TP}} + \hat{b}\hat{\sigma}^+_{\mathrm{TP}}). \quad (8)$$

D. Spin-torsion couplings

We now take into consideration the couplings between the mechanical torsional mode and the single N-V center. Before proceeding, we note that coherent interactions between N-V centers and several types of mechanical resonators have been studied [68,69]. These mechanical resonators include clamped cantilevers [70], optically trapped nanodiamond crystals [71–73], suspended carbon nanotubes [74], etc. In this setup, the single N-V center is positioned straight above the magnetized torsional cantilever, as shown in Fig. 3(a). When the nanomagnet rotates, the projection of the magnetic field along the spin component is changed, resulting in a magnetic coupling between the torsional mode and the N-V center. The strong magnetic coupling can be achieved by exquisite preparation of the dressed spin states.

A N-V center in diamond consists of a substitutional nitrogen atom replacing a carbon atom and an adjacent vacancy. The electronic ground states of a single N-V center are spin triplet states denoted as $|m_s = 0, \pm 1\rangle$ and the zero-field splitting D_{gs} between the degenerate sublevels $|m_s = \pm 1\rangle$ and $|m_s = 0\rangle$ is $2\pi \times 2.87$ GHz. For moderate applied magnetic fields, the static magnetic field $\vec{B}_z = B_z\vec{e}_z$ causes Zeeman splitting of the states $|m_s = \pm 1\rangle$, while the external microwave field $\vec{B}_{\mathrm{dr}} = B_0 \cos\omega_0 t \vec{e}_x$ polarized in the x direction drives the states $|m_s = 0\rangle$ and $|m_s = \pm 1\rangle$, as shown in Fig. 3(b). For convenience, we denote as the z axis the crystalline axis of the N-V center.

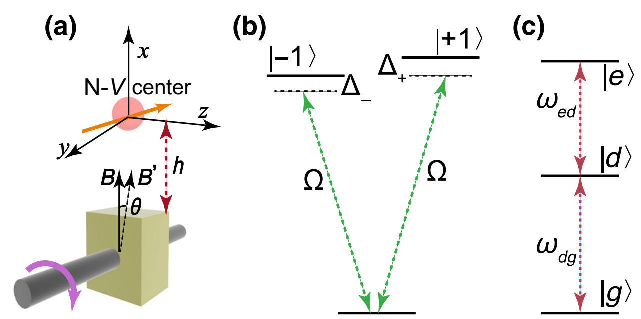

FIG. 3. Schematic design and level diagram of a single N-V center coupled to a magnetized torsional cantilever. (a) The N-V center is located straight above the magnetized torsional cantilever. The projection of the magnetic field along the spin component is changed if the torsional cantilever rotates, leading to the strong spin-torsion coupling. (b) Simplified energy levels of the N-V center in the electronic ground state $|^3A_2\rangle$. (c) Dressed spin states in the presence of external driving magnetic fields.

The magnetic field $\vec{B}_{\rm mg}(\theta)$ induced by the suspended nanomagnet depends on the angular displacement θ. We assume that the N-V center is placed in the position where $\vec{B}_{\rm mg}(\theta)$ is along the x axis, i.e., $\vec{B}_{\rm mg}(\theta) = B_{\rm mg}\cos\theta \cdot \vec{e}_x + B_{\rm mg}\sin\theta \cdot \vec{e}_z$, and $\theta \simeq 0$. Then, the interaction of the N-V center with the total magnetic fields (external driving and from the nanomagnet) can be described by

$$\hat{H}_{\text{N-}V} = \hbar D_{\rm gs}\hat{S}_z^2 + g_e\mu_B\{[\vec{B}_{\rm mg}(\theta) + \vec{B}_{\rm dr}]\cdot\hat{\vec{S}} + B_z\hat{S}_z\}, \quad (9)$$

where $g_e = 2$ is the N-V Landé factor, $\mu_B = 14$ MHz mT^{-1} is the Bohr magneton, and $\hat{\vec{S}} = (\hat{S}_x, \hat{S}_x, \hat{S}_z)$ is the spin operator of the N-V center. The motion of the torsional cantilever attached with the nanomagnet produces an angular and time-dependent magnetic field $\vec{B}_{\rm int}(\theta) \sim \partial_\theta \vec{B}_{\rm mg}(\theta)\hat{\theta}\cos\omega_m t$, which result in a spin-torsion coupling interaction $\hat{H}_{\rm int} = g_e\mu_B\vec{B}_{\rm int}(\theta)\cdot\hat{\vec{S}} \simeq \hbar\lambda(\hat{b}^\dagger + \hat{b})\hat{S}_z\cos\omega_m t$, where the coupling constant $\lambda = g_e\mu_B B_{\rm mg}\theta_{\rm ZPF}/\hbar$ is proportional to the magnetic field $B_{\rm mg}$ and the zero-point angular extension $\theta_{\rm ZPF}$. In the rotating frame at the frequency ω_m, we can acquire the Hamiltonian to describe the spin-torsion dynamics as follows:

$$\hat{H}_{\text{tor-N-}V} = \hbar\omega_m\hat{b}^\dagger\hat{b} + \hat{H}_{\text{N-}V} + \hbar\lambda(\hat{b}^\dagger + \hat{b})\hat{S}_z. \quad (10)$$

Note that the far-off resonant interactions between the N-V spin and the static and low-frequency components of magnetic fields along the x axis can be ignored. In the basis defined by the eigenstates of $\hat{S}_z$, i.e., $\{|m_s\rangle, m_s = 0, \pm1\}$, with $\hat{S}_z|m_s\rangle = m_s|m_s\rangle$, we have

$$\hat{H}_{\text{N-}V} = \sum_{m_s}[\hbar D_{\rm gs}m_s^2 + g_e\mu_B(B_z + B_{\rm mg}\sin\theta)m_s]|m_s\rangle\langle m_s| + \sum_{m_s m_{s'}} g_e\mu_B B_0\cos\omega_0 t\langle m_s|\hat{S}_x|m_s'\rangle|m_s\rangle\langle m_s'|, \quad (11)$$

where $\hat{S}_x = (\hbar/\sqrt{2})(|0\rangle\langle+1| + |0\rangle\langle-1| + \text{H.c.})$. In the rotating frame at the driving frequency ω_0 and under the rotating-wave approximation, we get

$$\hat{H}_{\text{N-}V} = \hbar\Delta_+|+1\rangle\langle+1| + \hbar\Delta_-|+1\rangle\langle+1| + \hbar\Omega(|-1\rangle\langle0| + |+1\rangle\langle0| + \text{H.c.}), \quad (12)$$

where $\hbar\Delta_\pm = \hbar D_{\rm gs} \pm g_e\mu_B(B_z \pm B_{\rm mg}\sin\theta) - \hbar\omega_0$ and $\hbar\Omega = (\sqrt{2}/4)g_e\mu_B B_0$.

In the following, we consider the symmetric detuning condition $\Delta_+ = \Delta_- = \Delta$ for simplicity (e.g., $B_z \to 0$). We now define the bright spin state $|b\rangle = (|+1\rangle + |-1\rangle)/\sqrt{2}$ and the dark spin state $|d\rangle = (|+1\rangle - |-1\rangle)/\sqrt{2}$. Then we find that the Hamiltonian (12) couples the state $|0\rangle$ to the bright state $|b\rangle$, while the dark state $|d\rangle$ remains decoupled. The resulting eigenstates of $\hat{H}_{\text{N-}V}$ are, therefore, given by $|d\rangle$ and two dressed states $|g\rangle = \cos(\alpha)|0\rangle - \sin(\alpha)|b\rangle$ and $|e\rangle = \sin(\alpha)|0\rangle + \cos(\alpha)|b\rangle$, with $\tan(2\alpha) = 2\sqrt{2}\Omega/\Delta$. The corresponding eigenfrequencies are given by $\omega_d = \Delta$, $\omega_{e/g} = (\Delta \pm \sqrt{\Delta^2 + 8\Omega^2})/2$, as illustrated in Fig. 3(c).

In the dressed-state basis $\{|g\rangle, |d\rangle, |e\rangle\}$, the Hamiltonian in Eq. (10) can be rewritten as

$$\hat{H}_{\text{tor-N-}V} = \hbar\omega_m\hat{b}^\dagger\hat{b} + \hbar\omega_{\rm eg}|e\rangle\langle e| + \hbar\omega_{\rm dg}|d\rangle\langle d| + \hbar(\lambda_g|g\rangle\langle d| + \lambda_e|d\rangle\langle e| + \text{H.c.})(\hat{b}^\dagger + \hat{b}), \quad (13)$$

where $\lambda_g = -\lambda\sin(\alpha)$ and $\lambda_e = \lambda\cos(\alpha)$. We further adjust the values of B_0 to drive the system to the resonance condition $\omega_{\rm ed} \simeq \omega_m \ll \omega_{\rm dg}$ and then the far-off-resonance state $|g\rangle$ can be neglected. Under the rotating-wave approximation, the spin-torsion dynamics can be described by the Jaynes-Cummings (JC) interaction Hamiltonian

$$\hat{H}_{\text{tor-N-}V} = \hbar\omega_m\hat{b}^\dagger\hat{b} + \hbar\omega_{\text{N-}V}\hat{\sigma}^z_{\text{N-}V} + \hbar\lambda_e(\hat{b}^\dagger\hat{\sigma}^-_{\text{N-}V} + \hat{b}\hat{\sigma}^+_{\text{N-}V}), \quad (14)$$

where $\hat{\sigma}^-_{\text{N-}V} = |d\rangle\langle e|$, $\hat{\sigma}^+_{\text{N-}V} = |e\rangle\langle d|$, $\hat{\sigma}^z_{\text{N-}V} = |e\rangle\langle e| - |d\rangle\langle d|$ and $\omega_{\text{N-}V} = \omega_e - \omega_d$.

III. EXPERIMENTAL PARAMETERS

According to the Hamiltonian (8) and (14), the whole system can be described by

$$\hat{H}_{\rm sys} = \hbar\omega_{\rm TP}\hat{\sigma}^z_{\rm TP} + \hbar\omega_m\hat{b}^\dagger\hat{b} + \hbar\omega_{\text{N-}V}\hat{\sigma}^z_{\text{N-}V} - \hbar g(t)\hat{b}^\dagger\hat{\sigma}^-_{\rm TP} + \hbar\lambda_e(t)\hat{b}^\dagger\hat{\sigma}^-_{\text{N-}V} + \text{H.c.} \quad (15)$$

The first three terms describe the free Hamiltonian of the system, while the last four terms describe two JC interactions: one between the torsional mode and the topological qubit and the other between the torsional mode and the single N-V center. As the torsional cantilever couples to the Majorana qubit and the N-V center simultaneously, it is possible to work as a quantum interface for quantum-state conversion.

Let us discuss the dynamics of the system in a realistic situation. For this setup, the relaxation (Γ_1) and dephasing (Γ_2) of the Majorana qubit, the decay of the mechanical resonator (γ_m), and also the dephasing of the N-V center (γ_s) should be taken into consideration. As a result, the full dynamics of this system can be described by the following master equation:

$$\frac{d\hat{\rho}(t)}{dt} = -\frac{i}{\hbar}[\hat{H}_{\rm sys}, \hat{\rho}] + \gamma_s\mathcal{D}(\hat{\sigma}^z_{\text{N-}V}) + \Gamma_1\mathcal{D}(\hat{\sigma}^-_{\rm TP}) + \Gamma_2\mathcal{D}(\hat{\sigma}^+_{\rm TP}\hat{\sigma}^-_{\rm TP}) + (n_{\rm th}+1)\gamma_m\mathcal{D}(\hat{b}) + n_{\rm th}\gamma_m\mathcal{D}(\hat{b}^\dagger), \quad (16)$$

where $n_{\rm th} = (e^{\hbar\omega_m/k_BT} - 1)^{-1}$ is the thermal phonon number at the environment temperature T and $\mathcal{D}(\hat{o}) = \hat{o}\hat{\rho}\hat{o}^\dagger - \frac{1}{2}\hat{o}^\dagger\hat{o}\hat{\rho} - \frac{1}{2}\hat{\rho}\hat{o}^\dagger\hat{o}$ for a given operator $\hat{o}$.

We now consider the experimental feasibility of our scheme and the appropriate parameters to achieve strong couplings. This manuscript employs the magnetized torsional cantilever to interface the Majorana qubit and the conventional spin qubit. As an alternative, one may also use the edge states of topological insulators or the planar Josephson junctions [75] to realize the Majorana qubit, which requires weaker magnetic fields. For the magnetized torsional cantilever, the nanomagnet suspended on the single-walled nanotube has a size of $80 \times 40 \times 20$ nm^3 and a moment of inertia of $I \sim 4.8 \times 10^{-33}$ kg m^2 with respect to the tube axis [76]. Then the torsional cantilever has a resonance frequency $\omega_m = [\frac{1}{2\pi}][(K/I)^{1/2}] \sim 2\pi \times 4$ MHz, and an angle of zero-point fluctuations $\theta_{\rm ZPF} = (\hbar^2/KI)^{1/4} \sim 3 \times 10^{-5}$, with $K \sim 3 \times 10^{-18}$ Nm per radian the torsional spring constant of the tube axis. As shown in Fig. 2(c), the topology-torsion coupling energy is about $E_m(\theta \simeq 0) \sim 42$ μ eV, which implies a coupling constant $g \sim 2\pi \times 200$ kHz. Moreover, the spin-torsion coupling can be modified by the distance between the torsional cantilever and the N-V center. For a distance $h \sim 80$ nm, one can obtain $B_{\rm mg} \sim 80$ mT [77] and $\lambda_e \sim 2\pi \times 200$ kHz.

We now take the decoherence processes of the system into consideration. In practical situations, the relaxation and dephasing rates of a Majorana qubit are strongly dependent on the concrete realization. Here, we take $\Gamma_1 \simeq \Gamma_2 \sim 2\pi \times 10$ kHz [58,78]. When it comes to the mechanical damping, the recent fabrication of carbon nanotube resonators can possess quality factors exceeding 10^5. For a torsional cantilever with $\omega_m \sim 2\pi \times 4$ MHz, the mechanical damping rate is about $\gamma_m = \omega_m/Q \sim 2\pi \times 40$ Hz, and the thermal phonon occupation number is about $n_{\rm th} \sim 104$ at the temperature of $T \sim 20$ mK. As for the N-V center, the dephasing time T_2 as long as several milliseconds can be reached in ultrapure diamond [79]. Here, we take $\gamma_s \sim 2\pi \times 2$ kHz. Finally, with these realistic parameters, we perform numerical simulations for the quantum dynamics of the system by solving the master equation, Eq. (16). As shown in Fig. 4, the coherent interactions can dominate the decoherence processes in this hybrid quantum device, which enables the system to enter the strong coupling regime.

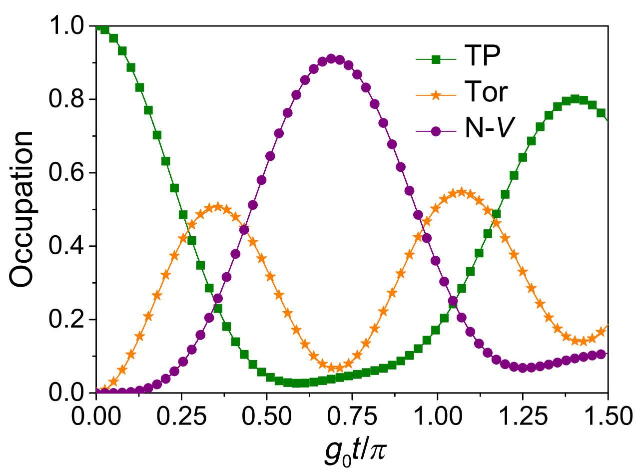

FIG. 4. Rabi oscillations of the hybrid tripartite system interfacing a topological qubit (TP) and a single N-V center (N-V) via a magnetized torsional cantilever (Tor). The topological qubit is initially in state $|1\rangle$, while the torsional mode is initially in the ground state and the N-V center in the state $|d\rangle$. We consider the system in a realistic case, with the coupling parameters $g = \lambda_g = g_0 \sim 2\pi \times 200$ kHz and the decay parameters $\Gamma_1 = \Gamma_2 = 0.05g_0$, $\gamma_m = 0.0002g_0$, $n_{\rm th} = 104$, and $\gamma_s = 0.1g_0$.

IV. DARK-STATE CONVERSION

In the previous sections, it is shown that the magnetized torsional cantilever can be employed as an intermediary to link the topological qubit and the single N-V center. Utilizing this quantum interface, one of the applications is to transfer the quantum state from the topological qubit to the spin qubit. The efficiency of the transformation relies on the specific protocol for quantum-state conversion. To transfer the quantum state in this setup, we show that both the direct-transfer scheme and the dark-state protocol are available.

As shown in Eq. (15), this hybrid tripartite system can be modeled by a beam-splitter Hamiltonian composed of two JC interactions. Therefore, we can use the JC interactions for quantum-state conversion. In particular, this direct-transfer scheme usually includes two steps. Step 1 is to turn on the topology-torsion couplings g for a time $t_1 = \pi/2g$ (while $\lambda_e = 0$), to transfer the quantum state from the Majorana qubit to the torsional mode. Step 2 is to turn off g and turn on the spin-torsion couplings λ_e for a time $t_2 = \pi/2\lambda_e$ (while $g = 0$), to map the quantum state from the torsional mode to the spin qubit. Note that this direct-transfer scheme has been studied in an optomechanical system [80]. In our setup, the topology-torsion couplings g can be controlled by the electrostatic gates [58], while the spin-torsion couplings λ_e can be controlled by the external driving fields.

As the direct-transfer scheme may suffer from decoherence of the mechanical mode, here we propose to realize the coherent quantum state conversion via a dark-state protocol [81–83]. This dark-state protocol is particularly robust against mechanical dissipations, as it is decoupled from the vibrational mode. We proceed by assuming that $\omega_m \simeq \omega_{\rm TP} \simeq \omega_{\text{N-}V}$. To describe quasiparticles formed by combinations of spin and Majorana excitations, we now introduce two polariton operators

$\hat{c}_{\rm br} = \sin(\beta)\hat{\sigma}^-_{\rm TP} + \cos(\beta)\hat{\sigma}^-_{\text{N-}V}$, and $\hat{c}_{\rm dk} = -\cos(\beta)\hat{\sigma}^-_{\rm TP} + \sin(\beta)\hat{\sigma}^-_{\text{N-}V}$, with $\tan(\beta) = -g/\lambda_e$. Then, one can verify that the Hamiltonian (15) can take a compact form,

$$\hat{H}_{\rm sys} = \hbar\tilde{\omega}_+\hat{c}^\dagger_+\hat{c}_+ + \hbar\tilde{\omega}_-\hat{c}^\dagger_-\hat{c}_- + \hbar\tilde{\omega}_{\rm dk}\hat{c}^\dagger_{\rm dk}\hat{c}_{\rm dk}, \qquad (17)$$

where $\hat{c}_\pm = (1/\sqrt{2})(\hat{c}_{\rm br} \pm \hat{b})$ describes polarons formed by combinations of polariton and phonon excitations. The corresponding frequencies of the polarons are $\tilde{\omega}_d = \omega_m$, $\tilde{\omega}_\pm = \omega_m \pm \sqrt{\lambda_e^2 + g^2}$. We refer to $\hat{c}_{\rm dk}$ as the mechanically dark polariton operator, as it involves the spin and Majorana operations only, decoupled from the torsional mode.

The excitation of $\hat{c}_{\rm dk}$ means that the system remains in the mechanically dark state. Utilizing the adiabatic evolution of the dark state, we can transfer the quantum state from the topological qubit to the single N-V center. In particular, in the limit $\beta = 0$, we get $\hat{c}_{\rm dk} = -\hat{\sigma}^-_{\rm TP}$, while in the limit $\beta = \pi/2$, we get $\hat{c}_{\rm dk} = \hat{\sigma}^-_{\text{N-}V}$. This result implies that if we adiabatically rotate the mixing angle β from zero to $\pi/2$, the mechanically dark polariton $\hat{c}_{\rm dk}$ would evolve from $-\hat{\sigma}^-_{\rm TP}$ to $\hat{\sigma}^-_{\text{N-}V}$. At the same time, the quantum state of the topological qubit could be transferred to the spin qubit except for a phase factor $e^{-i\pi}$.

Similar to the well-known stimulated Raman adiabatic passage, the dark-state protocol can be implemented by an adiabatic passage approach. To transfer the quantum state from the topological qubit to the N-V center, we initially make $\lambda_e(t)$ larger than $g(t)$, but keep $g(t)$ finite. Then, we modulate the coupling parameters carefully so that the dark polariton operator evolves adiabatically from $-\hat{\sigma}^-_{\rm TP}$ at the beginning to $\hat{\sigma}^-_{\text{N-}V}$ at the end. Meanwhile, the quantum state of the topological qubit will be transferred to the N-V center as the system evolves. To satisfy the adiabatic conditions, one needs to modulate the coupling strengths slowly to ensure that the system adiabatically follows the dark polaritons.

We perform numerical simulations for the dark-state protocol by solving the master equation, Eq. (16), with the Hamiltonian in Eq. (15), where the coupling parameters $g(t) = g_0 e^{-(t-\pi)^2/30}$, $\lambda_e(t) = 1.5 g_0 e^{-t^2/6}$, and $g_0 \sim 2\pi \times$ 200 kHz as discussed in Sec. III. To test the robustness of the protocol, we consider two kinds of initial states for the topological qubit: a Fock state $|1\rangle$ as displayed in Figs. 5(a) and 5(b), and a superposition state $\frac{1}{\sqrt{2}}|0\rangle + \frac{1}{\sqrt{2}}|1\rangle$, as displayed in Figs. 5(c) and 5(d). For the ideal case without decoherence, high fidelities 0.96 and 0.99 can be reached, as shown in Figs. 5(a) and 5(c). We find that, as the system evolves, the quantum states of the topological qubit are slowly transferred to the N-V center spin in the conversion process. Then, when it turns to the realistic case, high fidelities 0.83 and 0.93 can be reached, as shown in Figs. 5(b) and 5(d). Therefore, this dark-state protocol works very well in practical conditions.

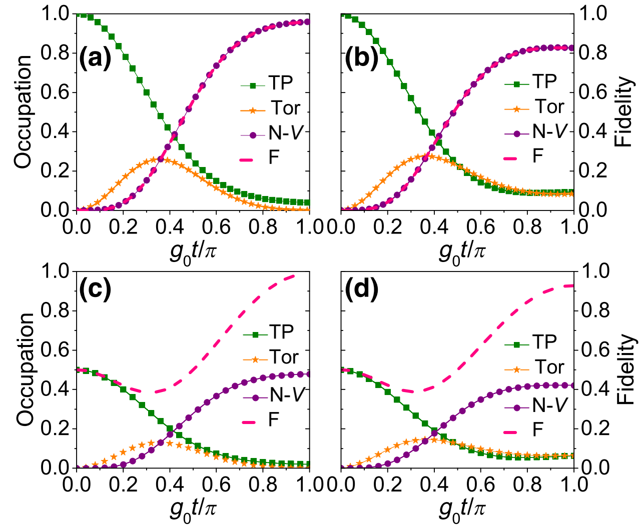

FIG. 5. Fidelity (F) and occupations (TP, Tor, N-V) as a function of time in the dark-state protocol, with the coupling parameters $g(t) = g_0 e^{-(t-\pi)^2/30}$ and $\lambda_e(t) = 1.5 g_0 e^{-t^2/6}$. Two kinds of initial states are under consideration: (i) a Fock state $|1\rangle$ in (a),(b) and (ii) a superposition state $1/\sqrt{2}|0\rangle + 1/\sqrt{2}|1\rangle$ in (c),(d). The decoherence parameters for (a),(c) are chosen as $\Gamma_1 = \Gamma_2 = \gamma_m = \gamma_s = 0$ and for (b),(d) $\Gamma_1 = \Gamma_2 = 0.05 g_0$, $\gamma_m = 0.0002 g_0$, $n_{\rm th} = 104$, and $\gamma_s = 0.1 g_0$.

V. CONCLUSIONS

In summary, we present a hybrid quantum device interfacing a topological qubit and a single N-V center via a high-Q magnetized torsional cantilever. We show that the mechanical torsional mode can strongly couple to the Majorana qubit and the single N-V center simultaneously and then we interface them for quantum-state conversion. In particular, the topology-torsion couplings are induced by the spin currents passing through the TNT junction, while the spin-torsion couplings can be realized by the exquisite preparation of dressed spin states and using a suspended nanomagnet. We also find that, under resonance conditions, one eigenstate of the system is the mechanically dark state, which provides a dark-state protocol for quantum-state conversion with very high fidelities. As the mechanical mode remains unpopulated during the conversion process, this dark-state scheme is extremely robust against mechanical damping. This hybrid quantum architecture integrated with the topological qubits and N-V spins provides a potential platform for quantum-information processing.

ACKNOWLEDGMENTS

B.L. thanks Di-Hao Sun and Shuai Li for fruitful discussions. This work is supported by the NSFC under Grants No. 11774285, No. 91536115, and No. 11534008 and the Fundamental Research Funds for the Central Universities.

Parts of the simulations are coded in Python using the Qutip library [84].

[1] S. R. Elliott and M. Franz, Colloquium: Majorana fermions in nuclear, particle, and solid-state physics, Rev. Mod. Phys. **87**, 137 (2015).

[2] R. M. Lutchyn, E. P. A. M. Bakkers, L. P. Kouwenhoven, P. Krogstrup, C. M. Marcus, and Y. Oreg, Majorana zero modes in superconductor csemiconductor heterostructures, Nat. Rev. Mater. **3**, 52 (2018).

[3] H. Zhang *et al.*, Quantized Majorana conductance, Nature **556**, 74 (2018).

[4] F. Wilczek, Majorana returns, Nature Phys. **5**, 614 (2009).

[5] D. Litinski and F. von Oppen, Quantum computing with Majorana fermion codes, Phys. Rev. B **97**, 205404 (2018).

[6] N. Read and D. Green, Paired states of fermions in two dimensions with breaking of parity and time-reversal symmetries and the fractional quantum Hall effect, Phys. Rev. B **61**, 10267 (2000).

[7] L. Fu and C. L. Kane, Superconducting Proximity Effect and Majorana Fermions at the Surface of a Topological Insulator, Phys. Rev. Lett. **100**, 096407 (2008).

[8] C. Nayak, S. H. Simon, A. Stern, M. Freedman, and S. Das Sarma, Non-abelian anyons and topological quantum computation, Rev. Mod. Phys. **80**, 1083 (2008).

[9] J. D. Sau, R. M. Lutchyn, S. Tewari, and S. Das Sarma, Generic New Platform for Topological Quantum Computation using Semiconductor Heterostructures, Phys. Rev. Lett. **104**, 040502 (2010).

[10] J. Alicea, Majorana fermions in a tunable semiconductor device, Phys. Rev. B **81**, 125318 (2010).

[11] R. M. Lutchyn, J. D. Sau, and S. Das Sarma, Majorana Fermions and a Topological Phase Transition in Semiconductor-Superconductor Heterostructures, Phys. Rev. Lett. **105**, 077001 (2010).

[12] L. Chen, W. LiMing, J.-H. Huang, C.-P. Yin, and Z.-Y. Xue, Majorana zero modes on a one-dimensional chain for quantum computation, Phys. Rev. A **90**, 012323 (2014).

[13] Y. Oreg, G. Refael, and F. von Oppen, Helical Liquids and Majorana Bound States in Quantum Wires, Phys. Rev. Lett. **105**, 177002 (2010).

[14] V. Mourik, K. Zuo, S. M. Frolov, S. R. Plissard, E. P. A. M. Bakkers, and L. P. Kouwenhoven, Signatures of Majorana fermions in hybrid superconductor-semiconductor nanowire devices, Science **336**, 1003 (2012).

[15] M. T. Deng, C. L. Yu, G. Y. Huang, M. Larsson, P. Caroff, and H. Q. Xu, Anomalous zero-bias conductance peak in a Nb-InSb nanowire-Nb hybrid device, Nano Lett. **12**, 6414 (2012).

[16] A. Das, Y. Ronen, Y. Most, Y. Oreg, M. Heiblum, and H. Shtrikman, Zero-bias peaks and splitting in an Al-InAs nanowire topological superconductor as a signature of Majorana fermions, Nat. Phys. **8**, 887 (2012).

[17] L. P. Rokhinson, X. Liu, and J. K. Furdyna, The fractional a.c. Josephson effect in a semiconductor-superconductor nanowire as a signature of Majorana particles, Nat. Phys. **8**, 795 (2012).

[18] F. Hassler, A. R. Akhmerov, C.-Y. Hou, and C. W. J. Beenakker, Anyonic interferometry without anyons: How a flux qubit can read out a topological qubit, New J. Phys. **12**, 125002 (2010).

[19] Z.-Y. Xue, S.-L. Zhu, J.-Q. You, and Z.-D. Wang, Implementing topological quantum manipulation with superconducting circuits, Phys. Rev. A **79**, 040303 (2009).

[20] K. Flensberg, Non-Abelian Operations on Majorana Fermions Via Single-Charge Control, Phys. Rev. Lett. **106**, 090503 (2011).

[21] M. Leijnse and K. Flensberg, Quantum Information Transfer between Topological and Spin Qubit Systems, Phys. Rev. Lett. **107**, 210502 (2011).

[22] S. Hoffman, C. Schrade, J. Klinovaja, and D. Loss, Universal quantum computation with hybrid spin-Majorana qubits, Phys. Rev. B **94**, 045316 (2016).

[23] S. Plugge, L. A. Landau, E. Sela, A. Altland, K. Flensberg, and R. Egger, Roadmapto Majorana surface codes, Phys. Rev. B **94**, 174514 (2016).

[24] Z.-T. Zhang and Y. Yu, Processing quantum information in a hybrid topological qubit and superconducting flux qubit system, Phys. Rev. A **87**, 032327 (2013).

[25] Z.-Y. Xue, L. B. Shao, Y. Hu, S.-L. Zhu, and Z. D. Wang, Tunable interfaces for realizing universal quantum computation with topological qubits, Phys. Rev. A **88**, 024303 (2013).

[26] F.-Y. Hong, H.-Q. Qian, J.-L. Fu, Z.-Y. Zhu, and L.-Z. Jiang, Strong coupling between a topological qubit and a nanomechanical resonator, Phys. Rev. A **87**, 032339 (2013).

[27] L. Jiang, C. L. Kane, and J. Preskill, Interface between Topological and Superconducting Qubits, Phys. Rev. Lett. **106**, 130504 (2011).

[28] P. Bonderson and R. M. Lutchyn, Topological Quantum Buses: Coherent Quantum Information Transfer between Topological and Conventional Qubits, Phys. Rev. Lett. **106**, 130505 (2011).

[29] S. Vishveshwara, A bit of both, Nature Phys. **7**, 450 (2011).

[30] C. Ohm and F. Hassler, Majorana fermions coupled to electromagnetic radiation, New J. Phys. **16**, 015009 (2014).

[31] A. Cottet, T. Kontos, and B. Douçcot, Squeezing light with Majorana fermions, Phys. Rev. B **88**, 195415 (2013).

[32] Z.-Y. Xue, M. Gong, J. Liu, Y. Hu, S.-L. Zhu, and Z. D. Wang, Robust interface between flying and topological qubits, Sci. Rep. **5**, 12233 (2015).

[33] M. W. Doherty, N. B. Manson, P. Delaney, F. Jelezko, J. Wrachtrup, and L. C. L. Hollenberg, The nitrogen-vacancy colour centre in diamond, Phys. Rep. **528**, 1 (2013).

[34] S. Hong, M. S. Grinolds, P. Maletinsky, R. L. Walsworth, M. D. Lukin, and A. Yacoby, Coherent, mechanicalcontrol of a single electronic spin, Nano. Lett. **12**, 3920 (2012).

[35] N. Bar-Gill, L. M. Pham, A. Jarmola, D. Budker, and R. L. Walsworth, Solid-state electronic spin coherence time approaching one second, Nat. Commun. **4**, 1743 (2013).

[36] K.-Y. Xia and J. Twamley, Generating spin squeezing states and Greenberger-Horne-Zeilinger entanglement using a hybrid phonon-spin ensemble in diamond, Phys. Rev. B **94**, 205118 (2016).

[37] W. L. Yang, Y. Hu, Z. Q. Yin, Z. J. Deng, and M. Feng, Entanglement of nitrogen-vacancy-center ensembles using

transmission line resonators and a superconducting phase qubit, Phys. Rev. A **83**, 022302 (2011).
[38] X.-X. Li, P.-B. Li, S.-L. Ma, and F.-L. Li, Preparing entangled states between two NV centers via the damping of nanomechanical resonators, Sci. Rep. **7**, 14116 (2017).
[39] Y. Zhou, S.-L. Ma, B. Li, X.-X. Li, F.-L. Li, and P.-B. Li, Simulating the Lipkin-Meshkov-Glick model in a hybrid quantum system, Phys. Rev. A **96**, 062333 (2017).
[40] Z.-Q. Yin, T.-C. Li, X. Zhang, and L.-M. Duan, Large quantum superpositions of a levitated nanodiamond through spin-optomechanical coupling, Phys. Rev. A **88**, 033614 (2013).
[41] Q. Chen, W.-L. Yang, M. Feng, and J.-F. Du, Entangling separate nitrogen-vacancy centers in a scalable fashion via coupling to microtoroidal resonators, Phys. Rev. A **83**, 054305 (2011).
[42] C. Zu, W.-B. Wang, L. He, W.-G. Zhang, C.-Y. Dai, F. Wang, and L.-M. Duan, Experimental realization of universal geometric quantum gates with solid-state spins, Nature **514**, 72 (2014).
[43] X.-K. Xu, Z.-X. Wang, C.-K. Duan, P. Huang, P.-F. Wang, Y. Wang, N.-Y. Xu, X. Kong, F.-Z. Shi, X. Rong, and J.-F. Du, Coherence-Protected Quantum Gate by Continuous Dynamical Decoupling in Diamond, Phys. Rev. Lett. **109**, 070502 (2012).
[44] L.-H. Dong, X. Rong, J.-P. Geng, F.-Z. Shi, Z.-K. Li, C.-K. Duan, and J.-F. Du, Scalable quantum computation scheme based on quantum-actuated nuclear-spin decoherence-free qubits, Phys. Rev. B **96**, 205149 (2017).
[45] P.-H. Cao, R. Betzholz, S.-L. Zhang, and J.-M. Cai, Entangling distant solid-state spins via thermal phonons, Phys. Rev. B **96**, 245418 (2017).
[46] T. Li, A. Miranowicz, X.-D. Hu, K.-Y. Xia, and F. Nori, Quantum memory and gates using a Λ-type quantum emitter coupled to a chiral waveguide, Phys. Rev. A **97**, 062318 (2018).
[47] K.-Y. Xia and J. Twamley, Solid-state optical interconnect between distant superconducting quantum chips, Phys. Rev. A **91**, 042307 (2015).
[48] W. L. Yang, Z. Q. Yin, Y. Hu, M. Feng, and J. F. Du, High-fidelity quantum memory using nitrogen-vacancy center ensemble for hybrid quantum computation, Phys. Rev. A **84**, 010301 (2011).
[49] X.-Y. Lü, Z.-L. Xiang, W. Cui, J. Q. You, and F. Nori, Quantum memory using a hybrid circuit with flux qubits and nitrogen-vacancy centers, Phys. Rev. A **88**, 012329 (2013).
[50] B. Li, P.-B. Li, Y. Zhou, S.-L. Ma, and F.-L. Li, Quantum microwave-optical interface with nitrogen-vacancy centers in diamond, Phys. Rev. A **96**, 032342 (2017).
[51] Z.-L. Xiang, X.-Y. Lü, T.-F. Li, J. Q. You, and F. Nori, Hybrid quantum circuit consisting of a superconducting flux qubit coupled to a spin ensemble and a transmission-line resonator, Phys. Rev. B **87**, 144516 (2013).
[52] J.-B. You, W.-L. Yang, Z.-Y. Xu, A. H. Chan, and C. H. Oh, Phase transition of light in circuit-QED lattices coupled to nitrogen-vacancy centers in diamond, Phys. Rev. B **90**, 195112 (2014).
[53] A. A. Kovalev, A. De, and K. Shtengel, Spin Transfer of Quantum Information between Majorana Modes and a Resonator, Phys. Rev. Lett. **112**, 106402 (2014).
[54] H. A. Kastrup, Quantization of the canonically conjugate pair angle and orbital angular momentum, Phys. Rev. A **73**, 052104 (2006).
[55] L. Jiang, D. Pekker, J. Alicea, G. Refael, Y. Oreg, A. Brataas, and F. von Oppen, Magneto-Josephson effects in junctions with Majorana bound states, Phys. Rev. B **87**, 075438 (2013).
[56] L. Jiang, D. Pekker, J. Alicea, G. Refael, Y. Oreg, and F. von Oppen, Unconventional Josephson Signatures of Majorana Bound States, Phys. Rev. Lett. **107**, 236401 (2011).
[57] P. Kotetes, G. Schön, and A. Shnirman, Engineering and manipulating topological qubits in 1D quantum wires, J. Korean Phys. Soc. **62**, 1558 (2013).
[58] J. Alicea, Y. Oreg, G. Refael, F. von Oppen, and M. P. A. Fisher, Non-abelian statistics and topological quantum information processing in 1D wire networks, Nat. Phys. **7**, 412 (2011).
[59] S. Vijay, T. H. Hsieh, and L. Fu, Majorana Fermion Surface Code for Universal Quantum Computation, Phys. Rev. X **5**, 041038 (2015).
[60] A. Saket, S. R. Hassan, and R. Shankar, Manipulating unpaired Majorana fermions in a quantum spin chain, Phys. Rev. B **82**, 174409 (2010).
[61] X.-J. Liu and P. D. Drummond, Manipulating Majorana fermions in one-dimensional spin-orbit-coupled atomic Fermi gases, Phys. Rev. A **86**, 035602 (2012).
[62] X.-J. Liu and A. M. Lobos, Manipulating Majorana fermions in quantum nanowires with broken inversion symmetry, Phys. Rev. B **87**, 060504 (2013).
[63] D. Sticlet, C. Bena, and P. Simon, Josephson effect in superconducting wires supporting multiple Majorana edge states, Phys. Rev. B **87**, 104509 (2013).
[64] H.-J. Kwon, K. Sengupta, and V. M. Yakovenko, Fractional ac Josephson effect in p-and d-wave superconductors, Eur. Phys. J. B **37**, 349 (2004).
[65] D.-H. Sun and J. Liu, Quench dynamics of the Josephson current in a topological Josephson junction, Phys. Rev. B **97**, 035311 (2018).
[66] S. Das Sarma, J. D. Sau, and T. D. Stanescu, Splitting of thezero-bias conductance peak as smoking gun evidence for the existence of the Majorana mode in a superconductor semiconductor nanowire, Phys. Rev. B **86**, 220506 (2012).
[67] F. Pientka, L. Jiang, D. Pekker, J. Alicea, G. Refael, Y. Oreg, and F. von Oppen, Magneto-Josephson effects and Majorana bound states in quantum wires, New J. Phys. **15**, 115001 (2013).
[68] Z.-Q. Yin, N. Zhao, and T.-C. Li, Hybrid opto-mechanical systems with nitrogen-vacancy centers, Sci. China: Phys., Mech. Astron. **58**, 1 (2015).
[69] P.-B. Li and F. Nori, Hybrid Quantum System with Nitrogen-Vacancy Centers in Diamond Coupled to Surface-Phonon Polaritons in Piezomagnetic Superlattices, Phys. Rev. Appl. **10**, 024011 (2018).
[70] P. Rabl, P. Cappellaro, M. V. Gurudev Dutt, L. Jiang, J. R. Maze, and M. D. Lukin, Strong magnetic coupling between an electronic spin qubit and a mechanical resonator, Phys. Rev. B **79**, 041302 (2009).

[71] Y. Ma, T. M. Hoang, M. Gong, T.-C. Li, and Z.-Q. Yin, Proposal for quantum many-body simulation and torsional matter-wave interferometry with a levitated nanodiamond, Phys. Rev. A **96**, 023827 (2017).
[72] T. Delord, L. Nicolas, Y. Chassagneux, and G. Hétet, Strong coupling between a single nitrogen-vacancy spin and the rotational mode of diamonds levitating in an ion trap, Phys. Rev. A **96**, 063810 (2017).
[73] T. M. Hoang, J. Ahn, J. Bang, and T.-C. Li, Electron spin control of optically levitated nanodiamonds in vacuum, Nat. Commun. **7**, 12250 (2016).
[74] P.-B. Li, Z.-L. Xiang, P. Rabl, and F. Nori, Hybrid Quantum Device with Nitrogen-Vacancy Centers in Diamond Coupled to Carbon Nanotubes, Phys. Rev. Lett. **117**, 015502 (2016).
[75] A. Fornieri, A. M. Whiticar, F. Setiawan, E. P. Marín, A. C. C. Drachmann, A. Keselman, S. Gronin, C. Thomas, T. Wang, R. Kallaher, G. C. Gardner, E. Berg, M. J. Manfra, A. Stern, C. M. Marcus, and F. Nichele, Evidence of topological superconductivity in planar Josephson junctions, arXiv:1809.03037.
[76] J. C. Meyer, M. Paillet, and S. Roth, Single-molecule torsional pendulum, Science **309**, 1539 (2005).
[77] H. J. Mamin, M. Poggio, C. L. Degen, and D. Rugar, Nuclear magnetic resonance imaging with 90-nm resolution, Nat. Nanotechnol. **2**, 301 (2007).
[78] A. Romito, J. Alicea, G. Refael, and F. von Oppen, Manipulating Majorana fermions using supercurrents, Phys. Rev. B **85**, 020502 (2012).
[79] P. L. Stanwix, L. M. Pham, J. R. Maze, D. Le Sage, T. K. Yeung, P. Cappellaro, P. R. Hemmer, A. Yacoby, M. D. Lukin, and R. L. Walsworth, Coherence of nitrogen-vacancy electronic spin ensembles in diamond, Phys. Rev. B **82**, 201201 (2010).
[80] L. Tian and H.-L. Wang, Optical wavelength conversion of quantum states with optomechanics, Phys. Rev. A **82**, 053806 (2010).
[81] Y.-D. Wang and A. A. Clerk, Using Interference for High Fidelity Quantum State Transfer in Optomechanics, Phys. Rev. Lett. **108**, 153603 (2012).
[82] L. Tian, Adiabatic State Conversion and Pulse Transmission in Optomechanical Systems, Phys. Rev. Lett. **108**, 153604 (2012).
[83] P.-B. Li, Y.-C. Liu, S.-Y. Gao, Z.-L. Xiang, P. Rabl, Y.-F. Xiao, and F.-L. Li, Hybrid Quantum Device based on NV Centers in Diamond Nanomechanical Resonators Plus Superconducting Waveguide Cavities, Phys. Rev. Appl. **4**, 044003 (2015).
[84] J. R. Johansson, P. D. Nation, and F. Nori, Qutip 2: A python framework for the dynamics of open quantum systems, Comput. Phys. Commun. **184**, 1234 (2013).